

LETTER TO THE EDITOR

V363 Cas: a new lithium rich Galactic Cepheid.[★]

G. Catanzaro¹, V. Ripepi², G. Clementini³, F. Cusano², G. De Somma², S. Leccia², M. Marconi²,
R. Molinaro², M. I. Moretti², I. Musella², and V. Testa⁴

¹ INAF-Osservatorio Astrofisico di Catania, Via S.Sofia 78, 95123, Catania, Italy
e-mail: giovanni.catanzaro@inaf.it

² INAF-Osservatorio Astronomico di Capodimonte, Salita Moiariello 16, 80131, Naples, Italy
e-mail: vincenzo.ripepi@inaf.it

³ INAF-Osservatorio di Astrofisica e Scienza dello Spazio, Via Gobetti 93/3, I-40129 Bologna, Italy

⁴ INAF – Osservatorio Astronomico di Roma, via Frascati 33, I-00078 Monte Porzio Catone, Italy

ABSTRACT

Context. Classical Cepheids (DCEPs) are important astrophysical objects not only as standard candles in the determination of the cosmic distance ladder, but also as a testbed for the stellar evolution theory, thanks to the strict connection between their pulsation [period(s), amplitudes] and stellar (luminosity, mass, effective temperature, metallicity) parameters.

Aims. We aim at unveiling the nature of the Galactic DCEP V363 Cas and other DCEPs showing cosmic abundances of lithium in their atmospheres.

Methods. We have collected three epochs high-resolution spectroscopy for V363 Cas with HARPS-N@TNG. Accurate stellar parameters: effective temperatures, gravities, microturbulences, radial velocities, and metal abundances were measured for this star.

Results. We detected a lithium abundance of $A(\text{Li}) = 2.86 \pm 0.10$ dex, along with iron, carbon and oxygen abundances of $[\text{Fe}/\text{H}] = -0.30 \pm 0.12$ dex, $[\text{C}/\text{H}] = -0.06 \pm 0.15$ dex and $[\text{O}/\text{H}] = 0.00 \pm 0.12$ dex. V363 Cas is the fifth among the Milky Way DCEPs to exhibit a Li-rich feature. An analysis of historical time-series spanning a hundred year interval shows that the period of V363 Cas is increasing, with a sharp acceleration after HJD = 2453000. This is a clear hint of first crossing of the instability strip.

Conclusions. Our results favour the scenario in which the five Galactic Li-rich DCEPs are first-crossing the instability strip having had slowly-rotating progenitors during their main sequence phase.

Key words. Stars: variables: Cepheids – Stars: abundances – Stars: fundamental parameters – Stars: individual: V363 Cas

1. Introduction

Among Classical Cepheids (DCEPs), the primary Population I standard candle within the Local Group, the shortest period DCEPs are likely associated with the first crossing of the instability strip (IS) and are expected to show peculiar chemical features, if compared with canonical, more evolved blue loop pulsators.

In this letter we report the discovery of a new rare lithium-rich DCEP. Only four DCEPs showing enhanced lithium abundance (via detection of the $\text{Li I } 6707.766 \text{ \AA}$) have been discovered in the Galaxy so far (Luck & Lambert 2011; Kovtyukh et al. 2016, 2019) and an additional one was detected in the Large Magellanic Cloud (LMC, Luck & Lambert 1992). All these objects show a lithium abundance $A(\text{Li}) \sim 3.0$ dex, in contrast to the majority of the Galactic DCEPs, which show $A(\text{Li}) < 1.2$ dex (Luck & Lambert 2011). This discovery was surprising as Li is expected to be depleted by proton-capture after the first dredge-up (1DU) occurring at the beginning of the Red Giant Branch (RGB) phase (Iben 1967). A natural explanation is that these DCEPs are at their first crossing of the IS and their envelopes do not show the signature of nuclear processes occurred during

the Main Sequence (MS) phase. Indeed, according to Kovtyukh et al. (2019), at least three out of the four Milky Way (MW) Li-rich DCEPs also show abundances of the CNO species which are consistent with the solar values, i.e. not processed by the CN-cycle. However, the 1DU is not the only phenomenon capable of depleting lithium. Rotational mixing can in fact reduce the lithium abundance by a factor of a hundred in a fraction of the MS lifetime, for sufficiently fast rotating MS stars (e.g. Brott et al. 2011). This would then explain the scant number of Li-rich DCEPs. Indeed, as noted by Kovtyukh et al. (2019), about 80% of the DCEPs that are expected to be at their first crossing (about 5% of the total) are Li-depleted. Therefore it can be hypothesized that the progenitors of the Li-rich and Li-depleted DCEPs (B stars) were, respectively, slow and fast rotating stars, when on the MS. It is known that a fraction ($\sim 15\%$) of the B-stars show $v \sin i < 20 \text{ km/s}$ (Huang et al. 2010), while their large majority rotates much faster. It is thought that the slow rotators lose most of their angular momentum on the MS due to stellar winds enhanced by the rotation itself (Maeder & Meynet 2000), hence when they become DCEPs they show the moderate rotational velocities typical of these stars.

An additional feature of the Li-rich DCEPs is that they most frequently are multi-mode pulsators. Among the four MW Li-rich DCEPs, ASAS J075842-2536.1 and ASAS J131714-6605.0 both pulsate in the first and second overtone (DCEP_1O2O), V371 Per pulsates in the fundamental and first overtone

[★] Based on observations made with the Italian Telescopio Nazionale Galileo (TNG) operated by the Fundación Galileo Galilei (FGG) of the Istituto Nazionale di Astrofisica (INAF) at the Observatorio del Roque de los Muchachos (La Palma, Canary Islands, Spain).

(DCEP_F1O), whereas V1033 Cyg is only a fundamental mode (DCEP_F) pulsator. According to Kovtyukh et al. (2019), multi-mode DCEPs have a less efficient mixing in their envelope than DCEP_F, hence would preferentially tend to retain their Li.

Even if other more complex processes can address the presence of lithium in DCEPs (see Kovtyukh et al. 2019, for a detailed discussion), the basic mechanism to explain Li-rich DCEPs is their passage through the IS at the first crossing. This occurrence can be verified by measuring the rate of period change due to evolution along the Hertzsprung-Russell Diagram (HRD), as the period is expected to increase at the first and third crossing while decreasing at the second one (see e.g. Turner et al. 2006). The data available to date allowed Kovtyukh et al. (2019) to detect a quick period change in V1033 Cyg whereas they were insufficient to detect period changes in the other three MW DCEPs.

In the course of a large project devoted to measure the chemical abundance of a hundred un-characterized or newly discovered Galactic DCEPs, we obtained high-resolution spectroscopy for V363 Cas and discovered the presence of a deep Li I 6707.766 Å line in the spectra of this MW DCEP. V363 Cas has long been considered a fundamental mode (ab-type) RR Lyrae variable with period $P \sim 0.546$ days (e.g. Nowakowski 1988). However, Hajdu et al. (2009) showed that the star is in fact a multi-mode DCEP pulsating in the first (1O) and second (2O) overtone modes, with a period ratio of $P_2/P_1 \sim 0.801$, which is typical of such multimode DCEPs (see, e.g. Fig. 3 in Udalski et al. 2018). Nevertheless, a number of recent papers still erroneously considered V363 Cas as an RR Lyrae star (e.g. Dambis et al. 2013; Prudil et al. 2020). Furthermore, Kervella et al. (2019a,b) claimed that V363 Cas is a binary RR Lyrae with an upper limit $0.2 M_{\odot}$ low mass companion.

In the following we confirm Hajdu et al. (2009) classification of V363 Cas as a multi-mode DCEP, based on both the star position on the HRD and an analysis of the photometric time-series data available for the star.

2. Spectroscopic observations and data analysis

Multiphase spectroscopic observations of V363 Cas were obtained at the 3.5m Telescopio Nazionale Galileo (TNG) equipped with the HARPS-N instrument, in three nights, November 21, 26 and December 19, 2019. HARPS-N features an echelle spectrograph covering the wavelength range between 3830 to 6930 Å, with a spectral resolution $R=115,000$. The signal-to-noise ratio (SNR) varies from 50 to 100 at $\lambda = 5000$ Å. Main characteristics of V363 Cas are summarised in Table 1.

Reduction of all the spectra, which included bias subtraction, spectrum extraction, flat fielding and wavelength calibration, was performed using the HARPS reduction pipeline. Radial velocities were measured by cross-correlating each spectrum with a synthetic template, using the IRAF task *FXCOR* and excluding Balmer lines as well as wavelength ranges containing telluric lines. The IRAF package *RVCORRECT* was adopted to determine the heliocentric velocity, by correcting the spectra for the Earth's motion.

To measure the elemental abundances we first need to estimate main stellar atmospheric parameters such as the effective temperature (T_{eff}), surface gravity ($\log g$), microturbulent (ξ) and the total lines broadening, measured in our spectra equal to $15 \pm 1 \text{ km s}^{-1}$. A T_{eff} value for each spectrum of V363 Cas was estimated using the line depth ratios (LDRs) method (Kovtyukh & Gorlova 2000), which is commonly used in the literature for

Table 1. Main characteristics of V363 Cas. $\langle V \rangle$ is the intensity-averaged magnitude of the star.

<i>Gaia</i> ID	<i>l</i>	<i>b</i>	$\langle V \rangle$	$E(B - V)$
	°	°	mag	mag
429162271910068352	118.46	-02.217	10.550	0.437 ^a

Notes. a = Kervella et al. (2019b)

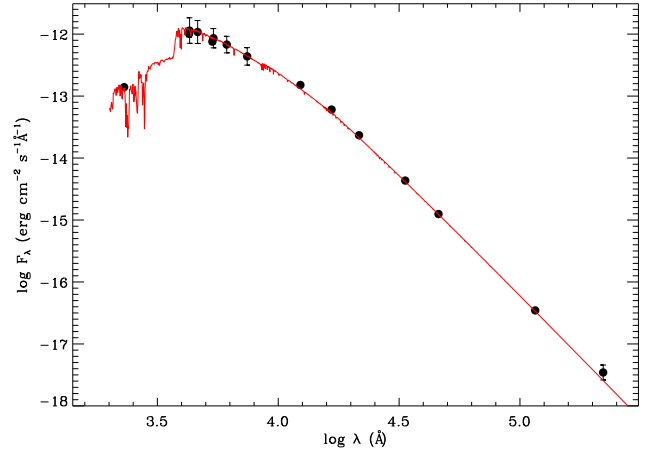


Fig. 1. Spectral energy distribution of V363 Cas. Filled dots represent the observed fluxes as retrieved from the VOSA tool. A red line shows the theoretical flux computed using the ATLAS9 model for $T_{\text{eff}} = 6660 \text{ K}$ and $\log g = 2.0$.

DCEPs. We measured about 32 LDRs in each spectrum. An iterative procedure was then applied to determine the microturbulent velocity ξ , iron abundance $[A(\text{Fe})]$ and surface gravity ($\log g$). ξ values were estimated by demanding the slope of the iron abundance as a function of the equivalent width (EW) to be null, that is, the iron abundance to not depend on EWs. To this purpose we used a sample of 145 Fe I spectral lines, extracted from the line list of Romaniello et al. (2008). The iron content was estimated by converting the measured EWs into abundances through the WIDTH9 code (Kurucz & Avrett 1981), after generating an appropriate model atmosphere with the ATLAS9 LTE code (Kurucz 1993a,b). At this stage, we neglected the $\log g$, as the Fe I lines are insensitive to this parameter. EWs were measured using an IDL¹ semi-automatic custom routine which allowed us to minimize errors in the continuum evaluation on the wings of the spectral lines. Then, we estimated the surface gravity by imposing the ionization balance between Fe I and Fe II lines. For the Fe II, we used a list of 24 lines extracted from the compilation by Romaniello et al. (2008). The atmospheric parameters derived for each spectrum of V363 Cas are summarized in Table 2. Since we obtained consistent temperatures and gravities for each night, we adopted the weighted average values, i.e. $T_{\text{eff}} = 6660 \pm 100 \text{ K}$ and $\log g = 2.0 \pm 0.1$, to reproduce the observed spectral energy distribution (SED) with the synthetic flux computed using the ATLAS9 code. The observed flux was retrieved from the VOSA tool (Bayo et al. 2008) and corrected for reddening adopting $E(B - V) = 0.437 \text{ mag}$ (Kervella et al. 2019b) and the Fitzpatrick (1999) extinction law. The comparison between observed and the theoretical SEDs is shown in Fig. 1. Furthermore, using the distance inferred from the *Gaia* DR2 paral-

¹ IDL (Interactive Data Language) is a registered trademark of Harris Geospatial Solutions

Table 2. Atmospheric parameters. For each spectrum of V363 Cas we list: heliocentric julian date (HJD) at mid exposure (column 1), pulsation phase (column 2), effective temperature (column 3), gravity (column 4), microturbulent and radial velocities (columns 5 and 6), iron and lithium abundances (column 7 and 8) expressed in a logarithmic scale relative to hydrogen.

HJD 2400000+	Phase	T_{eff} (K)	$\log g$	ξ (km s ⁻¹)	v_{rad} (km s ⁻¹)	A(Fe)	A(Li)
58809.5196	0.996	6650 ± 170	1.9 ± 0.2	2.1 ± 0.6	-55.2 ± 0.1	7.24 ± 0.12	2.86 ± 0.10
58814.4665	0.046	6620 ± 180	2.0 ± 0.2	2.4 ± 0.6	-55.9 ± 0.1	7.19 ± 0.12	2.86 ± 0.10
58837.3996	0.002	6710 ± 160	2.2 ± 0.3	2.1 ± 0.5	-50.2 ± 0.1	7.28 ± 0.12	2.86 ± 0.10

Table 3. Elemental abundances of V363 Cas, expressed in terms of the solar abundances (Grevesse et al. 2010), for 26 chemical species we measured in our target. Columns labelled with N represents number of lines used in the analysis. Results were obtained from the spectrum acquired on November 26, 2019.

El	[El/H]	N	El	[El/H]	N
Li	1.76 ± 0.14	1	Mn	-0.55 ± 0.12	8
C	-0.06 ± 0.15	4	Fe	-0.30 ± 0.12	169
O	0.00 ± 0.12	2	Ni	-0.08 ± 0.11	14
Na	-0.11 ± 0.12	4	Cu	-0.40 ± 0.10	2
Mg	-0.06 ± 0.12	5	Zn	-0.22 ± 0.15	3
Al	-0.38 ± 0.15	2	Sr	0.16 ± 0.10	2
Si	-0.08 ± 0.14	10	Y	0.15 ± 0.10	3
S	0.06 ± 0.16	3	Zr	0.08 ± 0.15	3
Ca	0.00 ± 0.15	4	Ba	0.86 ± 0.16	5
Sc	-0.08 ± 0.10	3	La	0.33 ± 0.15	2
Ti	-0.06 ± 0.15	20	Ce	0.05 ± 0.15	1
V	-0.49 ± 0.17	5	Nd	0.02 ± 0.13	5
Cr	-0.12 ± 0.10	17	Sm	0.16 ± 0.14	4

lax ($\pi = 0.7669 \pm 0.0278$ mas, to which we applied a zero point correction of 0.049 mas Groenewegen 2018), we derived a bolometric luminosity of $L/L_{\odot} = 260 \pm 49$ for V363 Cas.

The atmospheric parameters listed in Table 2 were used as inputs for the abundance analysis which was performed following the procedures in Catanzaro et al. (2019). For the analysis we used the spectrum acquired on November, 26 2019 which is the one with the highest SNR (up to 100). The abundances of the 26 species we detected in this spectrum are provided in Table 3. In Fig. 2 we show the comparison between observed and synthetic spectra in four main spectral regions, namely, H β and H α (as a check for the effective temperature), the Mg I triplet (as a check for $\log g$), and the Li I 6708.766 Å line. For the synthesis of the Li I line, we took into account the hyperfine structure and the close Fe I 6708.282 Å line.

As a general trend, V363 Cas appears to be slightly metal poor, since the iron peak elements show underabundances with respect to the Sun composition (Grevesse et al. 2010). The low iron content, $[\text{Fe}/\text{H}] \approx -0.30$, is consistent with a previous estimate by Fernley & Barnes (1997) (-0.38). We paid particular attention to light elements involved in the first dredge up mixing, such as carbon, oxygen, and sodium². Carbon and oxygen abundances are in agreement with the solar values, while sodium is slightly under-abundant. The lithium line was reproduced with an abundance of $A(\text{Li}) = 2.86 \pm 0.10$. This value is in good agreement with results from the standard big bang nucleosynthesis theory, which predicts a lithium abundance of $A(\text{Li}) = 2.72 \pm 0.06$ dex (Cyburt et al. 2008).

² Unfortunately, we did not observe any N spectral lines in our spectral range.

3. Time-series analysis and period change

The light-curve of V363 Cas was studied in detail by Hajdu et al. (2009) who identified the true nature of DCEP of this source on the basis of the time-series data collected with the Integral Optical Monitoring Camera (Alfonso-Garzón et al. 2012, IOMC) available at the time (1120 epochs over 6 years of data). However, since the IOMC has continued to accumulate data, we retrieve all data available so far for V363 Cas and analyse them again. At present the IOMC dataset comprises 3661 epochs with HJD spanning the range 2452654-2458504 days, (that is, from January 2003 to January 2019). This excellently long time-series was analysed with the Period04 period search software (Lenz & Breger 2005). We first considered the whole time-series, obtaining approximately the same pulsation periods as found by Hajdu et al. (2009), but also detecting in the periodogram highly significant residual peaks around these values, a clear indication that the periods are not stable. We then subdivided the IOMC timeseries in six chunks covering approximately the same time span/number of epochs, to be able to derive the periods with sufficient precision and find possible changes. The result of this exercise is presented in Fig. 3 (blue filled circles) for the P1 pulsation mode, as the P2 mode has a too small amplitude to allow precise results. A clear change in period is seen along the 16 years spanned by the IOMC data, with a quick increase at HJD~2453000 days. To confirm these results, we searched the literature for additional time-series data, finding usable datasets from the Hipparcos mission (Perryman et al. 1997) and the All-Sky Automated Survey for Supernovae (Jayasinghe et al. 2018, ASAS-SN) surveys. Results from these datasets are plotted in red and cyan in Fig. 3. Additional insight into the V363 Cas period changes were finally found in Nowakowski (1988), who analysed historical series of maxima for this star, providing periods valid in different epochs (green filled circles in Fig. 3). We can thus conclude that V363 Cas is actually changing period, although at a rather slow rate, since overall its dominant period increased from $P1 = 0.546517 \pm 0.000013$ days to $P1 = 0.546597 \pm 0.000001$ days, i.e. 0.00008 days in 100 years, or $\dot{P}/P \sim 1.5 \times 10^{-6} \text{ year}^{-1}$. However, after HJD~2453000 days, the star had a sharp period increase corresponding to $\dot{P}/P \sim 1.0 \times 10^{-5} \text{ year}^{-1}$. This general trend is confirmed by the O-C data-set of V363 Cas in the GEOS RR Lyr database (Le Borgne et al. 2007).

To provide updated periods and moments of maximum light for V363 Cas, we performed a period search using only the four most recent chunks of the IOMC time-series dataset, as the periods inferred from them are found to be consistent to each other. Results from this procedure are summarised in Table 4 whereas the folded light curves are shown in Fig. 4.

4. Discussion and conclusions

The bolometric luminosity and effective temperature derived in our analysis, allows us to place V363 Cas on the HRD. This is

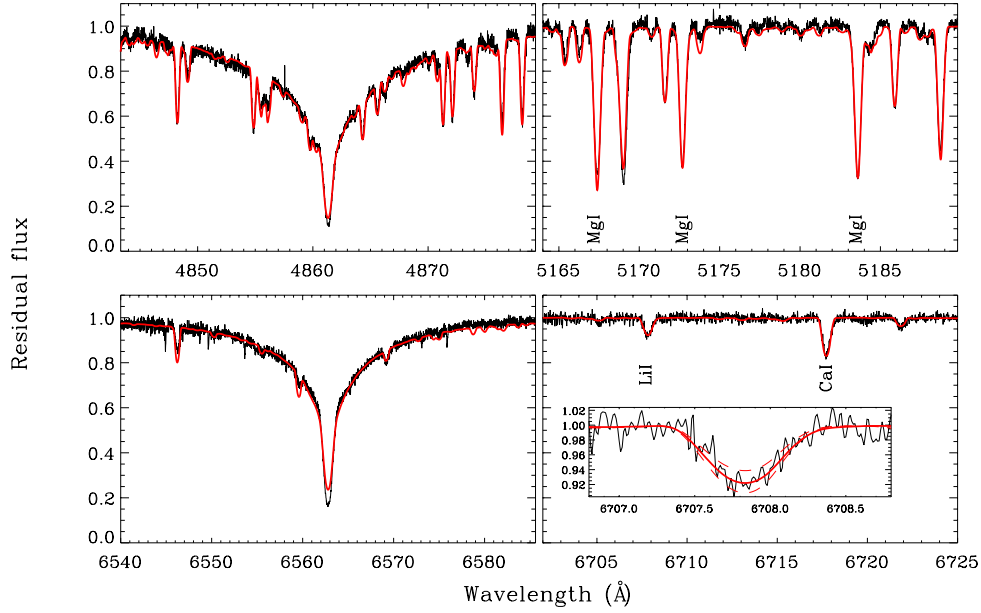


Fig. 2. Comparison between the spectrum of V363 Cas obtained on November 26, 2019 (black line) and the synthetic spectrum (red line) in four main spectral intervals centered, respectively, on $H\beta$ (top-left panel), the $Mg\ I$ triplet at $\lambda\lambda 5167.3216$, 5172.6843 , and 5183.6042 Å (top-right panel), $H\alpha$ (bottom-left panel) and the $Li\ I$ line at 6707.766 Å (bottom-right panel). In the insert, a solid red line shows the fit of the lithium line, while dashed lines represent limits for the experimental error ($\delta = \pm 0.1$ dex).

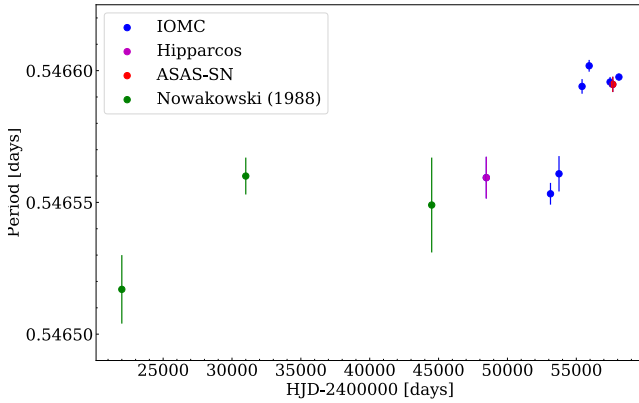


Fig. 3. Period change in the dominant pulsation mode (P1) of V363 Cas. Labels identify the sources of different literature datasets available for this star.

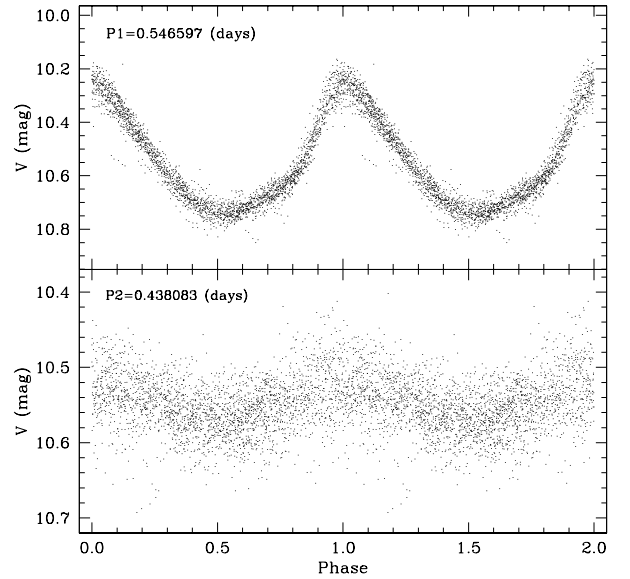


Fig. 4. Light curves of V363 Cas using only the IOMC dataset with HJD in the range of 2455202-2458504 days. Top and bottom panels show the 10 (P1) and 20 (P2) light curves, respectively.

shown in Fig. 5, where we have also plotted, for a comparison, the other four MW lithium-rich DCEPs. We adopted the T_{eff} values from Kovtyukh et al. (2019) for ASAS J075842-2536.1, ASAS J131714-6605.0 and V371 Per, while for V1033 Cyg we adopted the measure by Udovichenko et al. (2019). The luminosities were estimated by integrating the SEDs, which, as for V363 Cas, were calculated using the VOSA software. Figure 5 also displays in light grey the location of the sample of Galactic DCEPs recently analysed by Groenewegen (2020) together with the instability strip for DCEP_F and DCEP_10 of De Somma et al. (2020). Also plotted in Fig. 5 are the evolutionary tracks by Bressan et al. (2012) in the mass range $M=2.6-5.0 M_{\odot}$ for the chemical composition $Z=0.01$, $Y=0.267$ (which is adequate for V363 Cas and V371 Per) and $Z=0.014$ $Y=0.273$ (close to the present solar metal content $Z_{\odot}=0.0152$ and suitable for the remaining stars). V363 Cas is compatible with a mass of $\approx 3.2 M_{\odot}$ and is located at the blue side of the IS, as expected for a multi-mode DCEP pulsating in the 10O and 20O modes. In addition,

the absence of extended blue-loops in the tracks encompassing the position of V363 Cas, supports our suggestion that V363 Cas should be at its first crossing of the IS.

Takeda et al. (2013) carried out a spectroscopic study of 12 evolved DCEPs to the aim of investigating evolution-induced mixing in the envelope of these stars. They derived photospheric abundances of C (≈ -0.30), N ($\approx 0.4-0.5$), O (solar) and Na (≈ 0.2). Moreover, Li has been found to be very low in DCEPs ($A(\text{Li}) < 0.12$ Luck & Lambert 2011). V363 Cas shows almost solar values for both carbon and oxygen (no lines of N were detected in our spectral range) and a slight underabundance of

Table 4. Periods, peak-to-peak amplitudes in the V band and moment of maximum light (-2400000 days) of V363 Cas.

Mode	Period days	Amp(V) mag	HJD _{Max} days
P1	0.546597(1)	0.444	55201.435
P2	0.438083(2)	0.046	55201.57
P2/P1	0.80133(1)		

sodium (but still consistent with the solar value within the experimental errors). Regarding lithium, by spectral synthesis of the resonance line at 6707.766 \AA , we derived $A(\text{Li}) = 2.86 \pm 0.10$. This is consistent with the cosmic abundance and, at least, ≈ 1.8 dex over the average value found for DCEPs.

In summary, V363 Cas seems to possess all characteristic features of a first-crossing DCEP: it is Li-rich, has solar-like C(N)O abundances (reflecting the photospheric abundance during the MS phase) and shows an increasing period. The multi-mode nature of V363 Cas is also a common feature among the few known Li-rich MW DCEPs. Indeed, adding V363 Cas, 4 out of 5 known MW Li-rich DCEPs are found to pulsate in two modes. Additionally, 3 are 2O/1O pulsators whereas only one is a 1O/F (V371 Per) pulsator. In this respect, our results support Kovtyukh et al. (2019) hypothesis that inefficient mixing in the atmospheres of these DCEPs may have facilitated the preservation of Li. Regarding the position of the MW Li-rich DCEPs on the HRD, ASAS 075852-2536.1 appears to be a low-mass DCEP ($\approx 2.6 M_{\odot}$), V1033 Cyg is more massive ($\approx 4.4 M_{\odot}$) and is the only one which was shown to have an increasing period as we now have found also of V363 Cas. V371 Per ($\approx 4.6 M_{\odot}$) and ASAS 311714-6605.0 ($\approx 4.2 M_{\odot}$) are far from the blue loops according to their tracks. Hence, all these DCEPs are very likely at their first-crossing of the IS.

To conclude, the emerging scenario is that a Li-rich DCEP should necessarily be at its first crossing (to avoid mixing due to 1DUP) and should have had a low rotation velocity when on the MS (to avoid dilution by rotation mixing, see Brott et al. 2011). New high-resolution observations of MW DCEPs from our and other groups are ongoing. Therefore, more Li-rich DCEPs are likely to be discovered in the near future, increasing the statistics and helping to unveil the true nature of these stars.

Acknowledgements. This work has made use of data from the European Space Agency (ESA) mission *Gaia* (<https://www.cosmos.esa.int/gaia>), processed by the *Gaia* Data Processing and Analysis Consortium (DPAC, <https://www.cosmos.esa.int/web/gaia/dpac/consortium>). Funding for the DPAC has been provided by national institutions, in particular the institutions participating in the *Gaia* Multilateral Agreement. The Italian participation in DPAC has been supported by Istituto Nazionale di Astrofisica (INAF) and the Agenzia Spaziale Italiana (ASI) through grants I/037/08/0, I/058/10/0, 2014-025-R.0, and 2014-025-R.1.2015 to INAF (PI M.G. Lattanzi). We acknowledge partial support from the project "MITiC: Mining The Cosmos Big Data and Innovative Italian Technology for Frontier Astrophysics and Cosmology" (PI B. Garilli). This publication makes use of VOSA, developed under the Spanish Virtual Observatory project supported by the Spanish MINECO through grant AyA2017-84089. VOSA has been partially updated by using funding from the European Union's Horizon 2020 Research and Innovation Programme, under Grant Agreement n° 776403 (EXOPLANETS-A). This research has made use of the SIMBAD database, operated at CDS, Strasbourg, France.

References

Alfonso-Garzón, J., Domingo, A., Mas-Hesse, J. M., et al. 2012, *A&A*, 548, A79
 Bayo, A., Rodrigo, C., Barrado y Navascués, D., Solano, E., Gutiérrez, R., Morales-Calderón, M., Allard, F. 2008, *A&A* 492, 277B.

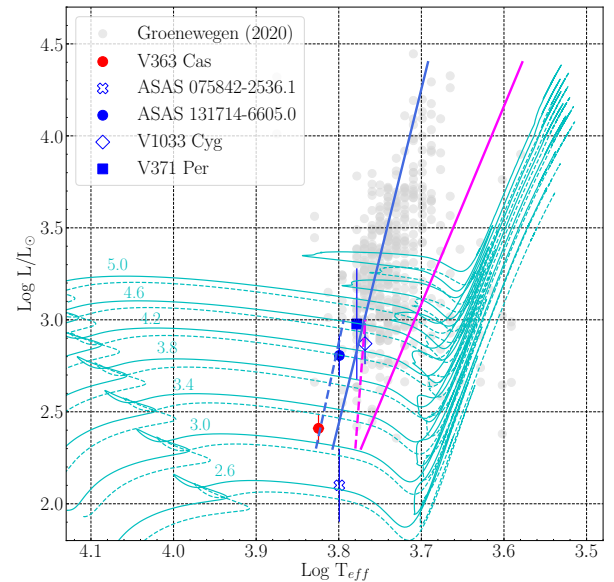


Fig. 5. HR diagram of the known MW Li-rich DCEPs. V363 Cas is the red filled circle. Different symbols (see labels) are used for the other 4 literature stars. The Li-normal DCEPs by Groenewegen (2020) are shown in light grey as a reference. Instability strips for DCEP_F (solid lines) and DCEP_1O (dashed lines) by De Somma et al. (2020) as well as evolutionary tracks by Bressan et al. (2012) for $Z=0.01$ $Y=0.267$ (solid cyan lines) and $Z=0.014$ $Y=0.273$ (dashed cyan lines) in the mass range 2.6 – $5.0 M_{\odot}$ are also over-plotted to the data.

- Bressan, A., Marigo, P., Girardi, L., et al. 2012, *MNRAS*, 427, 127
 Brott, I., de Mink, S. E., Cantiello, M., et al. 2011, *A&A*, 530, A115
 Catanzaro, G., Busá, I., Gangi M., Giarrusso, M., Leone, F., Munari, M., 2019, *MNRAS*, 484, 2530
 Cyburt R. H., Fields B. D., Olive K. A., 2008, *J. Cosmol. Astropart. Phys.*, 11, 12
 Dambis, A. K., Berdnikov, L. N., Kniazev, A. Y., et al. 2013, *MNRAS*, 435, 3206
 De Somma, G., Marconi, M., Molinaro, R., et al. 2020, *ApJS*, 247, 30
 Fernley, J., & Barnes, T. G. 1997, *A&AS*, 125, 313
 Fitzpatrick, E., 1999, *PASP*, 111, 63
 Grevesse N., Asplund M., Sauval A. J., Scott P., 2010, *Ap&SS*, 328, 179
 Groenewegen, M. A. T. 2018, *A&A*, 619, A8
 Groenewegen, M. A. T. 2020, *A&A*, 635, A33
 Hajdu, G., Jurcsik, J., & Sodor, A. 2009, *Information Bulletin on Variable Stars*, 5882, 1
 Huang, W., Gies, D. R., & McSwain, M. V. 2010, *ApJ*, 722, 605
 Iben, I. 1967, *ARA&A*, 5, 571
 Jayasinghe, T., Kochanek, C. S., Stanek, K. Z., et al. 2018, *MNRAS*, 477, 3145
 Kervella, P., Gallenne, A., Evans, N. R., et al. 2019a, *A&A*, 623, A117
 Kervella, P., Arenou, F., Mignard, F., et al. 2019b, *A&A*, 623, A72
 Kovtyukh, V. V., Gorlova, N. I. 2000, *A&A*, 358, 587
 Kovtyukh, V., Lemasle, B., Kniazev, A., et al. 2019, *MNRAS*, 488, 3211
 Kovtyukh, V., Lemasle, B., Chekhonadskikh, F., et al. 2016, *MNRAS*, 460, 2077
 Kurucz R.L., 1993, A new opacity-sampling model atmosphere program for arbitrary abundances. In: Peculiar versus normal phenomena in A-type and related stars, IAU Colloquium 138, M.M. Dworetzky, F. Castelli, R. Faraggiana (eds.), A.S.P. Conferences Series Vol. 44, p.87
 Kurucz R.L., 1993, Kurucz CD-ROM 13: ATLAS9, SAO, Cambridge, USA
 Kurucz R.L., Avrett E.H., 1981, *SAO Special Rep.*, 391
 Le Borgne, J. F., Paschke, A., Vandenbroere, J., et al. 2007, *A&A*, 476, 307
 Lenz, P., & Breger, M. 2005, *Communications in Asteroseismology*, 146, 53
 Luck, R. E., Lambert, D. L., 2011, *AJ*, 142, 136
 Luck, R. E., Lambert, D. L., 1992, *ApJS*, 79, 303
 Maeder, A., & Meynet, G. 2000, *ARA&A*, 38, 143
 Nowakowski J. 1988, *J. Am. Assoc. Variable star obs.*, 17, 7
 Perryman, M. A. C., Lindegren, L., Kovalevsky, J., et al. 1997, *A&A*, 500, 501
 Prudil, Z., Dékány, I., Grebel, E. K., et al. 2020, *MNRAS*, 492, 3408
 Romaniello, M., Primas, F., Mottini, M., et al. 2008, *A&A*, 488, 731
 Takeda, Y., Kang, D.-I., Han, I., Lee, B.-C., & Kim, K.-M., 2013, *MNRAS*, 432, 769
 Turner, D. G., Abdel-Sabour Abdel-Latif, M., & Berdnikov, L. N. 2006, *PASP*, 118, 410
 Udalski, A., Soszyński, I., Pietrukowicz, P., et al. 2018, *Acta Astron.*, 68, 315
 Udovichenko, S. N., Kovtyukh, V. V., & Keir, L. E. 2019, *Odessa Astronomical Publications*, 32, 83